

Stability of \mathcal{PT} and anti- \mathcal{PT} -symmetric Hamiltonians with multiple harmonicsJulia Cen^{1,*}, Yogesh N. Joglekar^{2,†} and Avadh Saxena^{1,‡}¹Theoretical Division and Center for Nonlinear Studies, Los Alamos National Laboratory, Los Alamos, New Mexico 87545, USA²Department of Physics, Indiana University-Purdue University Indianapolis, Indianapolis, Indiana 46202, USA

(Received 11 February 2023; revised 13 December 2023; accepted 10 January 2024; published 14 February 2024)

Hermitian Hamiltonians with time-periodic coefficients can be analyzed via Floquet theory, and have been extensively used for engineering Floquet Hamiltonians in standard quantum simulators. Generalized to non-Hermitian Hamiltonians, time periodicity offers avenues to engineer the landscape of Floquet quasienergies across the complex plane. We investigate two-level non-Hermitian \mathcal{PT} and anti- \mathcal{PT} -symmetric Hamiltonians with coefficients that have multiple harmonics using Floquet theory. By analytical and numerical calculations, we obtain their regions of stability, defined by real Floquet quasienergies, and contours of exceptional point (EP) degeneracies. We extend our analysis to study the phases that accompany these cyclic changes with the biorthogonality approach. Our results demonstrate that these time-periodic Hamiltonians generate a rich landscape of stable (real) and unstable (complex) regions.

DOI: [10.1103/PhysRevResearch.6.013167](https://doi.org/10.1103/PhysRevResearch.6.013167)

I. INTRODUCTION

Time-dependent Schrödinger equations are in general difficult to solve analytically, and usually one has to resort to using perturbation or numerical methods. One of the few analytically solvable time-dependent models is the Rabi model [1], which is a two-level system driven by an oscillatory classical field. Its key feature is that when the field frequency is close to the energy-level gap of the two-level system, the system undergoes complete population inversion at an arbitrarily small field strength. Following the Rabi model, Shirley developed a formalism for periodically driven systems using Floquet theory [2–4]. Over the years, there has been an increasing interest in studying time-periodic driven systems for applications in control and sensing. Examples can be found in the engineering of quantum materials [5], topological structures [6–8], controlling interwell tunneling of a Bose-Einstein condensate [9], and detecting low-frequency magnetic fields [10].

During the past quarter of a century, research on non-Hermitian systems incorporating parity-time inversion or \mathcal{PT} -symmetries has also seen tremendous growth [11,12]. Such open systems with balanced, spatiotemporally separated gain and loss are described by effective, non-Hermitian Hamiltonians H with \mathcal{PT} symmetry, $[H, \mathcal{PT}] = 0$ [13]. This antilinear symmetry implies that the Hamiltonian eigenvalues are either real or occur in complex-conjugate pairs, with the

\mathcal{PT} -symmetry breaking transition occurring at exceptional point (EP) degeneracies where corresponding eigenmodes also coalesce. These remarkable properties have allowed complex extensions of quantum theory [14–18]. The realization of \mathcal{PT} -symmetry as a pair of optical waveguides [19–22] further fueled the growth of work on the experimental side in a wide range of areas including unidirectional invisibility [23], electrical circuits [24–26], photonic lattices [27], mechanics [28], optical resonators [29], acoustics [30], as well as in minimal quantum systems [31–35].

A decade ago, new symmetry called anti- \mathcal{PT} -symmetry (\mathcal{APT} symmetry) was introduced in non-Hermitian systems and was realized as balanced negative and positive refractive index materials [36]. A system is said to have \mathcal{APT} symmetry if the \mathcal{PT} operator anticommutes with the Hamiltonian H' , i.e., $\{H', \mathcal{PT}\} = 0$. Although, *prima facie*, the two symmetries appear distinct, it is easy to check that H is \mathcal{PT} symmetric if and only if the Hamiltonian $H' = iH$ has the \mathcal{APT} symmetry. Such Hamiltonians have been realized in flying atoms [37], optical waveguides with imaginary couplings [38], optical four-wave mixing in cold atoms [39], Lorentz dynamics [40], diffusive systems [41], qubits [42], nonlinear dimers [43], and trapped ions [44,45].

When \mathcal{PT} symmetries were introduced for Floquet systems, this brought numerous novel phenomena that fundamentally arise due to the interplay between periodic gain-loss variation and oscillatory, unitary dynamics introduced by a static, Hermitian Hamiltonian. For \mathcal{PT} -symmetric Hamiltonians with a single drive—an oscillatory gain-loss term or an oscillatory Hermitian term, but not both—this led to a rich landscape of \mathcal{PT} symmetric, stable regions, and \mathcal{PT} broken unstable regions separated by contours of EPs. This landscape contains \mathcal{PT} -broken regions at vanishingly small gain-loss strengths, as well as \mathcal{PT} -symmetric regions at arbitrarily large gain-loss strengths, at specific modulation frequencies [46–48]. Non-Hermitian Floquet dynamics with \mathcal{PT}

*julia.cen@outlook.com

†yojoglek@iupui.edu

‡avadh@lanl.gov

symmetries have been investigated in ultracold atoms [49], nitrogen-vacancy (NV) centers [50], superconducting qubits [51,52], electrical circuits [53,54] and [55,56] which also includes systems without \mathcal{PT} symmetries. These extensive investigations, however, have been limited to single-frequency drives. Work on multitone drives has mainly been in the Hermitian setting, for instance, looking at realization of Floquet model as a Creutz ladder [57] and Floquet engineering in optical lattices [58]. The models explored are multifrequency drives in a single direction. We consider the effects of two noncommuting terms in the Hamiltonian with different harmonics in the non-Hermitian scenario, thereby distinguishing our work.

In particular, we investigate \mathcal{PT} -symmetric and \mathcal{APT} -symmetric Hamiltonians where the Hermitian or gain-loss terms have multiple harmonics, by using the Floquet formalism. We determine the stable (real Floquet eigenvalues) and unstable (complex conjugate Floquet eigenvalues) regions numerically by using the frequency-domain Floquet Hamiltonian H_F and analytically from eigenvalues of the nonunitary, one-period time-evolution operator $G(T) \equiv \exp(-iH_F T)$. Subsequently, we use the cyclic variations of the non-Hermitian Hamiltonians to obtain the biorthogonal Berry phase [59–61] for our models. The plan for the paper is as follows. In Sec. II we set out the formalism and establish the notation for both \mathcal{PT} -symmetric and \mathcal{APT} -symmetric models that we consider. We present the stability phase diagrams for the \mathcal{PT} -symmetric case, and discuss their common, salient features, followed by corresponding results for the \mathcal{APT} -symmetric models. In Sec. III, we present the results for the geometric phases acquired during cyclic variations. We conclude the paper with a brief discussion in Sec. IV.

II. FLOQUET FORMALISM

For a two-level system, a general Hamiltonian is given by $H(t) = \mathbf{A}(t) \cdot \boldsymbol{\sigma} + i\mathbf{B}(t) \cdot \boldsymbol{\sigma}$, where $\mathbf{A}(t)$, $\mathbf{B}(t)$ are real vectors and $\boldsymbol{\sigma} = (X, Y, Z)$ denotes the vector with the Pauli matrices. Since all 2×2 matrices are encoded here, the requisite anti-linear symmetry imposes a further constraint of $\mathbf{A} \cdot \mathbf{B} = 0$. We emphasize that since the Pauli matrices form an orthogonal basis for all 2×2 matrices, arbitrary \mathcal{PT} symmetric and \mathcal{APT} -symmetric Hamiltonians can be written in this form.

For a time-periodic Hamiltonian, the instantaneous eigenvalues $\lambda_k(t)$ of $H(t) = H(t + T)$ do not determine the dynamics. The long-term dynamics of the system, instead, are determined by the spectrum of the corresponding Floquet Hamiltonian $H_F = H(t) - i\partial_t$ ($\hbar = 1$), represented as an infinite-dimensional, nondiagonal matrix in the frequency space. If $H(t)$ contains sinusoidal time dependence, then the frequency-space Floquet Hamiltonian H_F is tridiagonal [46,47], whereas if $H(t)$ has piecewise constant entries with sharp changes, the matrix H_F has nonzero entries throughout. The spectrum of the Floquet Hamiltonian $H_F(\omega, \beta\omega)$, comprising Floquet quasienergies $\epsilon_{n\alpha} = \epsilon_\alpha + n\omega$, changes from purely real to complex conjugate pairs as a function of the non-Hermiticity strength γ and frequency $\omega \equiv 2\pi/T$ of modulation. An alternate method is to obtain the one-period time-evolution operator $G(T) = \mathbb{T} \exp(-i \int_0^T H(t') dt')$, where \mathbb{T} denotes time-ordered product that takes into account

the noncommuting nature of Hamiltonians at different instances of time. The 2×2 nonunitary operator $G(T)$ can also be used to define the Floquet Hamiltonian within the folded-zone scheme [46,47] with two Floquet eigenenergies ϵ_α . If one uses piecewise constant Hamiltonian $H(t)$, the operator $G(T)$ can be analytically calculated [51,62].

There are in total three nontrivial cases of \mathcal{PT} - and \mathcal{APT} -symmetric double-driven models, where by nontrivial we mean models with both stable and unstable regions, characterized by real and complex-conjugate Floquet quasienergies, respectively. Trivial cases are those with no finite threshold; one either has purely real or purely imaginary Floquet eigenvalues. In the following paragraphs, we will explore the salient features of each nontrivial case.

A. \mathcal{PT} -symmetric models

Without loss of generality, we consider \mathcal{PT} -symmetric models where \mathbf{A} is in the x - y plane while \mathbf{B} is along the z axis. We start with the following cosine- Y -cosine- Z driven model,

$$H(t) = JX + \gamma \{ \cos(\omega t)Y - i \cos(\beta\omega t)Z \}, \quad (1)$$

where an integer $\beta \geq 1$ denotes that the gain-loss term oscillates faster than the Hermitian term. In the following, we use $J = 1$ to set the energy scale, thereby using $\gamma \equiv \gamma/J$ and $\omega \equiv \omega/J$ to denote the dimensionless amplitude and frequency of the Floquet drive. For analytical calculations, we replace the cosine with a step function taking values ± 1 , thereby creating a sequence of constant Hamiltonians H_ℓ for the $1 \leq \ell \leq 4\beta$ equal intervals that span the period T . The piecewise constant Hamiltonians are given by

$$H_\ell = JX + \gamma(\mathbf{v}_y \cdot \mathbf{I})Y - i\gamma(\mathbf{v}_z \cdot \mathbf{I})Z, \quad (2)$$

$$\mathbf{v}_y = (\underbrace{1 \cdots 1}_\beta \underbrace{-1 \cdots -1}_{2\beta} \underbrace{1 \cdots 1}_\beta), \quad (3)$$

$$\mathbf{v}_z = (\underbrace{1, -1, -1, 1, \dots, 1, -1, -1, 1}_{\beta \text{ copies}}), \quad (4)$$

$$\mathbf{I} = (0, \dots, \underbrace{1}_{\ell \text{ th entry}}, \dots, 0). \quad (5)$$

Taking Hamiltonian (1) and utilizing Floquet theory, we are able to transform our time-dependent problem into an effective time-independent one in which we can find the Floquet quasienergies, and then obtain their phase diagrams. Constructing the corresponding piecewise version of the driven model (2) allows for analytical calculations to find the phase boundaries more commonly known as the exceptional lines, dividing unbroken (stable) and broken (unstable) \mathcal{PT} -symmetric regions. In the analytical approach, the time-evolution operator G is a 2×2 matrix, and therefore can always be written as $\exp(-iH_\ell T)$ where H_ℓ will be a 2×2 matrix. Then, every 2×2 matrix can be written as $\epsilon_0 I + \epsilon_F \mathbf{n}_F \cdot \boldsymbol{\sigma}$ where $\epsilon_\alpha = \pm \epsilon_F$ denote the two Floquet quasienergies, \mathbf{n}_F is a unit vector. Note that there is a nontrivial identity piece $\epsilon_0 = 1$ but one can show that $\epsilon_0(T) = 0$ or π . Similarly, by comparing the components of G versus the matrix expansion of $\exp(-iH_\ell T)$, one can get implicit equations for components \mathbf{n}_F and the value of ϵ_F . The reader can refer to [51], which has an example of such a calculation. Hence, the

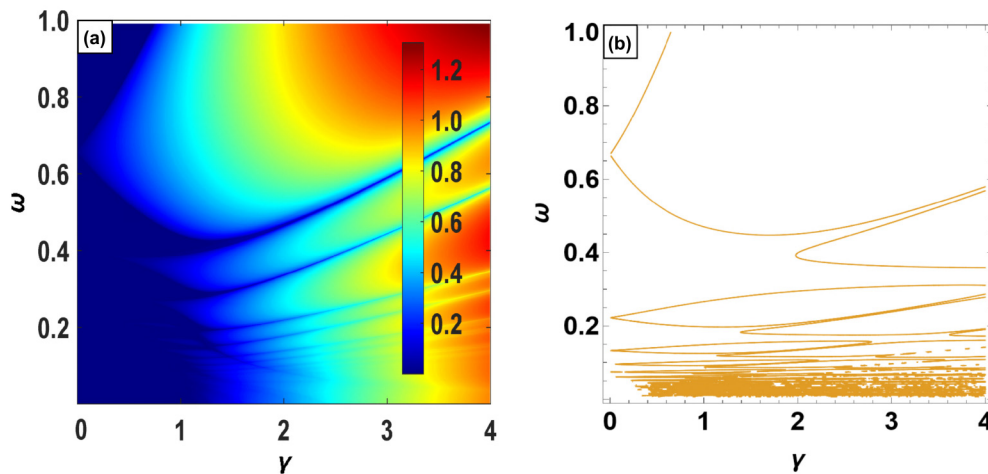


FIG. 1. Stability of doubly driven non-Hermitian Hamiltonian with $\beta = 3$. (a) Plot of $\max \text{Im} \epsilon_\alpha$ in the parameter space of ω and γ for Hamiltonian (1) shows stable deep-blue regions punctuated by unstable regions at $\gamma \ll 1$ at specific frequencies. The resonance at $\omega = 2J/\beta$ is clearly seen. (b) EP contours obtained from $G(T)$ for the piecewise constant Hamiltonian (2) also show qualitatively similar features, particularly at small γ values. Note that stable regions at large gain-loss strengths $\gamma \gg 1$ are more robust for the piecewise constant Hamiltonian, Eq. (2), than its continuous counterpart, Eq. (1).

single-period time evolution operator is given by

$$G(T) = \prod_{\ell=1}^{4\beta} e^{-iH_\ell T/4\beta}, \quad (6)$$

$$= \cos(\epsilon_F T) \mathbb{I}_2 - i \sin(\epsilon_F T) (\mathbf{n}_F \cdot \boldsymbol{\sigma}). \quad (7)$$

Under this parametrization, the reality of Floquet eigenvalues, which is also the requirement for stability, is equivalent to $|\cos(4\beta\epsilon_F\tau)| \leq 1$. The EP contours, thus, are given by $\cos(4\beta\epsilon_F\tau) = \pm 1$.

Figure 1 shows the representative results of such analysis. The left-hand panel, plotting the maximum imaginary part of Floquet quasienergies $\max \text{Im} \epsilon_\alpha(\omega, \gamma)$ for $\beta = 3$, shows deep blue stable regions ($\max \text{Im} \epsilon_\alpha = 0$) at small gain-loss strengths, punctuated by unstable, \mathcal{PT} -symmetry broken regions ($\max \text{Im} \epsilon_\alpha \neq 0$) that occur at vanishingly small γ when the modulation frequency ω takes specific values. We also see thin slivers of stable regions that extend to arbitrarily large gain-loss strengths $\gamma \gg 1$. These results are obtained from an 82×82 truncated-matrix $H_F(\omega, \beta\omega)$ but remain the same when the matrix size is doubled, thereby confirming that the results are valid in the infinite-Floquet-matrix limit. The right-hand panel shows the EP contours that are obtained from the analytical constraint $|\cos(\epsilon_F T)| = 1$. We have two main commonalities for small γ . At high frequencies, the two models reduce down to static models with averaged values for the drives, giving a good match for the main resonances. At low frequencies, in the $\omega = 0$ limit, piecewise and continuous models have matching potentials. The resonances/Arnold tongues are expected to match here, however, it is graphically hard to produce a perfect match due to the dense, thin nature of the Arnold tongues and numerical computation limits. On the other hand, the structure of the EP contours at moderate to large values of γ is different, although its salient features—such as the existence of \mathcal{PT} -symmetric, stable regions at arbitrarily large values of γ —are retained by the

analytically tractable model. Similar results are obtained for other integer values of β , and the phase diagram remains qualitatively similar for rational β s as well.

Resonances, where unstable regions emerge, come from the interference between the Hermitian and anti-Hermitian drive in Eq. (1). The rate at which the Arnold tongues in Fig. 1 decay depends on how constructive/destructive the interference of drives is. Our subsequent \mathcal{APT} -symmetric models have two anti-Hermitian drives and we will observe two primary resonances, one from each drive. This is a distinguishing feature of systems with different frequency drives. It is also important to point out that when $\beta = 1$, the time-dependent part of the Hamiltonian (1) is proportional to $(Y - iZ)$. Since the matrix $(Y - iZ)$ is defective, i.e., it has doubly degenerate zero eigenvalue with only one eigenvector, the eigenvalues of the corresponding Floquet Hamiltonian, with the static JX term, are always real. The nontrivial phase diagram, seen in Fig. 1 arises only when $\beta \neq 1$.

B. \mathcal{APT} -symmetric models

Next, we consider two nontrivial models that are best thought of as \mathcal{APT} symmetric, because they have two anti-Hermitian drives and a constant Hermitian term. We call them cosineX-cosineY and cosineX-sineY models. The sinusoidally varying Hamiltonians for the two cases are given by

$$H_{cc}(t) = i\gamma \{ \cos(\omega t)X + \cos(\beta\omega t)Y \} + JZ, \quad (8)$$

$$H_{cs}(t) = i\gamma \{ \cos(\omega t)X + \sin(\beta\omega t)Y \} + JZ. \quad (9)$$

As before, the analysis of the frequency-domain, truncated Floquet Hamiltonian $H_F(\omega, \beta\omega)$ is supplemented by analytical calculations using piecewise constant Hamiltonians $H_I = i\gamma \{ (\mathbf{v}_x \cdot \mathbf{I})X + (\mathbf{v}_y \cdot \mathbf{I})Y \} + JZ$. Here, the corresponding

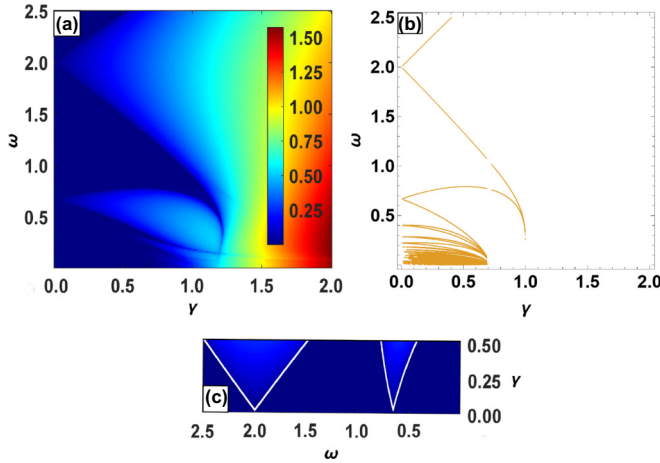


FIG. 2. Stability of cosineX-cosineY \mathcal{APT} -symmetric Hamiltonian, Eq. (8), with $\beta = 3$. (a) $\max \text{Im}\epsilon_\alpha(\gamma, \omega)$ shows triangular unstable regions near resonances $\omega = 2, 2/\beta$ and their subharmonics. (b) Corresponding EP contours from piecewise-constant Hamiltonian show same qualitative features, including the absence of stable regions at large gain-loss strengths. (c) Boundaries of the two main resonances from perturbation theory.

4β -dimensional vectors \mathbf{v}_k for the cosineX-cosineY model are given by

$$\mathbf{v}_x = (\underbrace{1 \cdots 1}_\beta \underbrace{-1 \cdots -1}_{2\beta} \underbrace{1 \cdots 1}_\beta), \quad (10)$$

$$\mathbf{v}_y = (\underbrace{1, -1, -1, 1, \dots, 1, -1, -1, 1}_{\beta \text{ copies}}), \quad (11)$$

and those for the cosineX-sineY model are given by

$$\mathbf{v}_x = (\underbrace{1 \cdots 1}_\beta \underbrace{-1 \cdots -1}_{2\beta} \underbrace{1 \cdots 1}_\beta), \quad (12)$$

$$\mathbf{v}_y = (\underbrace{1, 1, -1, -1, \dots, 1, 1, -1, -1}_{\beta \text{ copies}}). \quad (13)$$

Figure 2 shows representative results of such analysis for the Hamiltonian (8) with $\beta = 3$. The left-hand panel shows that $\max \text{Im}\epsilon_\alpha$ is zero at small $\gamma \ll 1$ except for the triangular regions of instability ($\max \text{Im}\epsilon_\alpha > 0$) that arise near resonances $\omega = 2J, \omega = 2J/\beta$, and their lower resonances. We also note, in contrast to the two-drive \mathcal{PT} -symmetric case, there are no regions of stability, with real Floquet eigenvalues, at large $\gamma \gg 1$. The right-hand panel in Fig. 2 shows the corresponding analytical EP contours, thereby confirming the salient, common features of cosineX-cosineY \mathcal{APT} -symmetric Hamiltonian. We note that a perturbation theory approach at small γ near the resonances can be used to obtain the slopes and corrections to linearity of the triangular unstable regions seen in Fig. 2(c) [46,47]. In particular, we compare the two main resonances $\omega = 2J$ from the effective Hamiltonian:

$$\begin{pmatrix} J - \frac{\gamma^2}{32J} & \frac{i\gamma}{2} \\ \frac{i\gamma}{2} & \omega - J + \frac{\gamma^2}{32J} \end{pmatrix}, \quad (14)$$

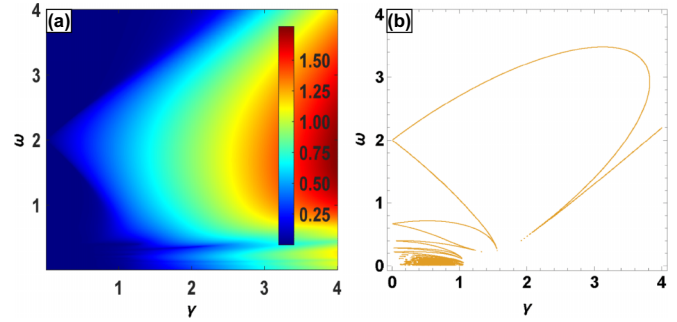


FIG. 3. Stability of cosineX-sineY Hamiltonian, Eq. (9), with $\beta = 3$. (a) $\max \text{Im}\epsilon_\alpha(\gamma, \omega)$ shows a large triangular unstable region near $\omega = 2$ and a small sliver near $\omega = 2/\beta$, along with their subharmonics. (b) Corresponding EP contours from piecewise-constant Hamiltonian show same qualitative features. The clustering of EP contours at low frequencies $\omega \ll 1$ to the static threshold $\gamma_{EP} = 1$ is also clear.

and $\omega = 2J/\beta$ from

$$\begin{pmatrix} J + 3\omega - \frac{11\gamma^2}{32J} & -\frac{\gamma}{2} \\ \frac{\gamma}{2} & 6\omega - J + \frac{11\gamma^2}{32J} \end{pmatrix}. \quad (15)$$

Results for the cosineX-sineY model, Eq. (9), are shown in Fig. 3. As in the previous cases, the stable regions, indicated by $\max \text{Im}\epsilon_\alpha = 0$ are seen at small gain-loss strengths except in the vicinity of primary resonance at $\omega = 2J$. The key features of the stability diagram are shared by the EP contours obtained from the piecewise-constant Hamiltonian model. In addition to the large, stable region at high frequencies and moderate gain-loss strengths, the cosineX-sineY model also includes clustering of the low-frequency domain EP contours to the static threshold value of $\gamma_{PT} = J$.

III. BERRY PHASES UNDER NON-HERMITIAN, CYCLIC DYNAMICS

In Hermitian systems, when the single-drive Rabi problem is generalized to two drives, the system Hamiltonian traces out a closed, two-dimensional loop in the parameter space. Berry phases result from the adiabatic evolution of eigenstates of the Hamiltonian on a closed cycle in the parameter space. The standard Berry-phase expression for Hermitian Hamiltonians is given by

$$\theta_{B\alpha} = i \int_0^T ds \langle \psi_\alpha(s) | \partial_s | \psi_\alpha(s) \rangle, \quad (16)$$

where the Hamiltonian $H(s) = H(s+T)$ has eigenstates $|\psi_\alpha(s)\rangle$ with eigenvalues $\epsilon_\alpha(s)$, and Eq. (16) is valid as long as the time T is much longer than inverse of the smallest energy gap $\min |\epsilon_m(s) - \epsilon_n(s)|$ [59–61]. Due to the unitary evolution generated by H , the eigenstates remain normalized, $\partial_s \langle \psi_\alpha(s) | \psi_\alpha(s) \rangle = 0$, and therefore the Berry phase defined in Eq. (16) is a real number.

One interesting feature of doubly driven non-Hermitian, Floquet models compared with single-driven ones is that we are now able to investigate the analog of Berry phases under cyclic evolution. Due to left and right eigenvectors that are

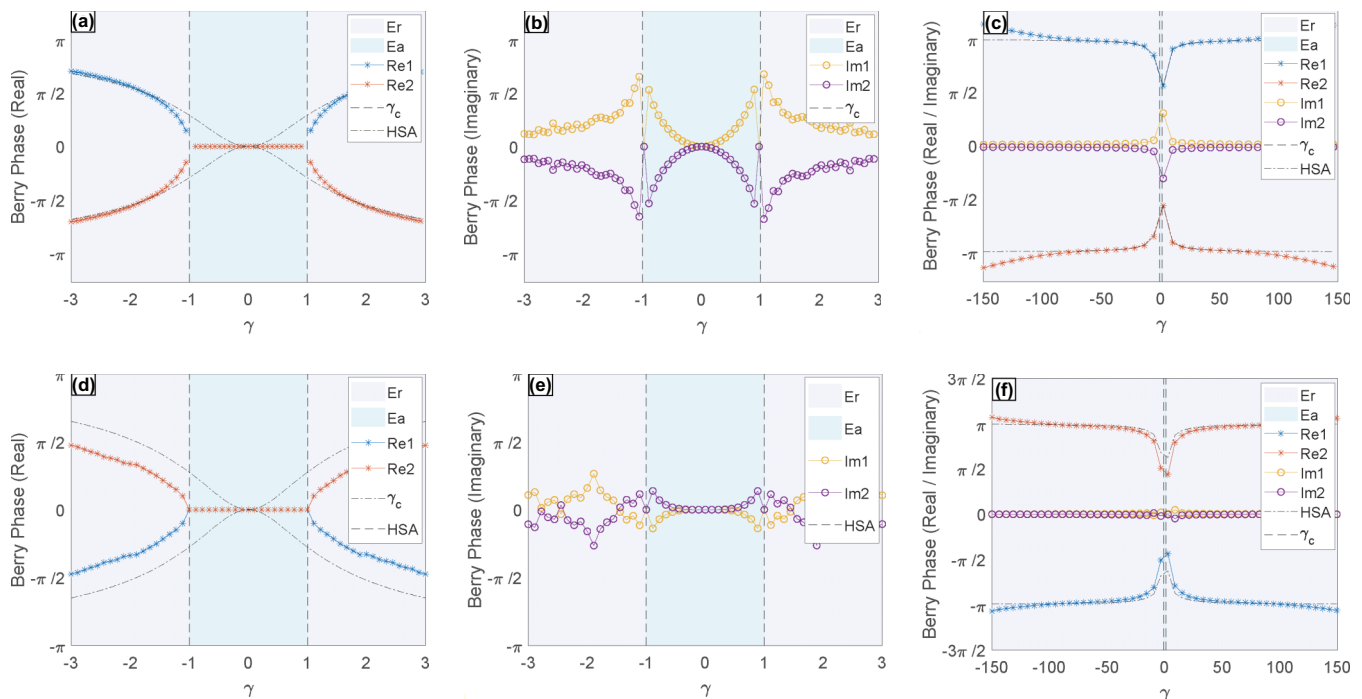


FIG. 4. Real and imaginary parts of the complex Berry phase, Eq. (17), for the non-Hermitian \mathcal{PT} -symmetric system (18). Er denotes the real eigenvalues region, Ea is alternating real-imaginary eigenvalues region and HSA is the abbreviation for “half the solid angle.” (a)–(c) Top panel shows results for $\beta = 1$, i.e., same frequency drives. Blue, red and orange, purple are the real and imaginary parts of the Berry phases from the two different initial eigenstates of the system. Black dash-dotted denote half the solid angle subtended by the closed curve evolved by the eigenstates. Here, $\gamma_c = \pm 1$ denotes the threshold above which the instantaneous eigenvalues become complex for some range of $s \sim T/4, 3T/4$. (d)–(f) Bottom panel shows corresponding results for $\beta = 3$.

not related by Hermitian conjugation, nonorthogonality of the (left) eigenstates of $H(s)$, the presence of EPs where the minimum energy gap vanishes, and the chiral mode switch that such systems undergo during cyclic evolution [50,52], the notion of Berry phases can be defined in several different ways. We use the biorthogonality approach, where the Berry phase for an eigenstate is defined by

$$\theta_{B\alpha} = i \int_0^T ds \langle \psi_{L\alpha}(s) | \partial_s | \psi_{R\alpha}(s) \rangle, \quad (17)$$

where $|\psi_{L\alpha}\rangle$ and $|\psi_{R\alpha}\rangle$ denote the biorthonormalized left and right eigenstates of the Hamiltonian $H(s)$ with eigenvalue ϵ_α [63–66]. In standard Hermitian quantum mechanics, we have a complete set of orthonormal eigenstates to give a well-defined Hilbert space. In the non-Hermitian scenario, because we do not have an orthogonal set of eigenstates, introducing biorthogonality creates a set of biorthogonal left and right eigenstates for its Hilbert and dual space, replacing orthogonality. Since the two eigenstates are not related by Hermitian conjugation, $\langle \psi_L | \neq | \psi_R \rangle^\dagger$, the quantity defined by Eq. (17) is a complex number, in general. The real part remains the Berry phase, and the imaginary part is the dissipative/growth effect from the non-Hermiticity of our models. Hence, we define the regions of real and complex Berry phases as stable and unstable, respectively. An example of realizing complex Berry phases has been shown in [65] with optical waveguides.

First, we consider the \mathcal{PT} -symmetric, cosineY-sineZ model with the Hamiltonian

$$H(s) = JX + \gamma \left[\cos\left(\frac{2\pi s}{T}\right)Y + i \sin\left(\frac{2\pi \beta s}{T}\right)Z \right]. \quad (18)$$

As previously, we use $J = 1$ as the relevant energy scale, and therefore $\gamma \equiv \gamma/J$ denotes the dimensionless strength of the sinusoidal modulation. The top panel in Fig. 4 shows the dependence of the complex Berry phase obtained from Eq. (17) as a function of γ at $\beta = 1$. Note that the instantaneous eigenvalues of $H(s)$, Eq. (18), are given by $\pm \sqrt{J^2 + \gamma^2 \cos(4\pi s/T)}$, and are therefore purely real when $|\gamma|/J \leq 1$. In contrast, for $|\gamma| > J$, the instantaneous eigenvalues become complex-conjugate pairs near $s = T/4, 3T/4$. The bottom panel in Fig. 4 shows the corresponding results for the complex Berry phase when $\beta = 3$. We see that although the behavior at large $|\gamma|/J \gg 1$ is the same in both double-drive cases, details at moderate values of $|\gamma|/J \sim O(1)$ are different. Furthermore, with the same frequencies, we can see that the real part of Berry phase tends to the value of half the solid angle very rapidly. For different frequencies, it never reaches the value of half the solid angle. Comparing the imaginary parts for the same frequencies, we observe they tend to zero in the real eigenvalues region, but oscillate for different frequencies.

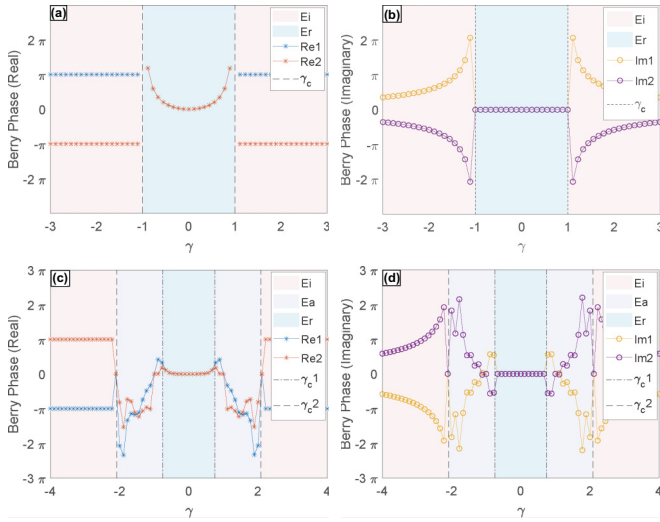


FIG. 5. Real and imaginary parts of the complex Berry phases $\theta_{B\alpha}$ for the \mathcal{AP} -symmetric Hamiltonian (19). E_r , E_a , HSA are as in Fig. 4, and E_i denote the imaginary eigenvalues region. (a), (b) Top panel shows results for $\beta = 1$, i.e., same frequency drives. Blue, red and orange, purple are the real and imaginary parts of the Berry phases from the two different initial eigenstates of the system. (c), (d) Bottom panel shows results for $\beta = 3$. Here, γ_c , γ_{c1} , γ_{c2} denote the transition of eigenvalue regions between real (blue region), pure imaginary (pink region), and alternating real and pure imaginary (purple region) cases.

Lastly, we consider an \mathcal{AP} -symmetric model with two anti-Hermitian drives,

$$H(s) = i\gamma \left[\cos\left(\frac{2\pi s}{T}\right)X + \sin\left(\frac{2\pi s}{T}\right)Y \right] + JZ. \quad (19)$$

When the drives are of the same frequency, $\beta = 1$, the instantaneous spectrum of Eq. (19) is real for $|\gamma|/J \leq 1$ while at larger drive strengths, $|\gamma|/J > 1$ the eigenvalues are complex conjugates. The top panel in Fig. 5 shows the real and imaginary parts of the complex Berry phase across the threshold $\gamma_c = \pm 1$ when $\beta = 1$. In this case, the anti-Hermitian drives sweep a circle and therefore we find that the real part of the Berry phase is fixed at $\pm\pi$ when $|\gamma|/J > 1$. On the other hand, for smaller drive strengths, the imaginary part of Eq. (17) is zero. The bottom panel in Fig. 5 shows corresponding results when $\beta = 3$. Once again, we see the common features where $\text{Re}\theta_{B\alpha} = \pm\pi$ when the instantaneous eigenvalues are complex conjugates, whereas $\text{Im}\theta_{B\alpha} = 0$ when they are purely real. In addition, different frequencies introduce a new eigenvalue region, E_a , of alternating real-imaginary values. Here, Berry phases are again complex conjugates, with more jagged changes.

IV. DISCUSSION

In this paper, we have analyzed the stability of several \mathcal{PT} and \mathcal{AP} -symmetric, non-Hermitian Hamiltonians with multiple harmonics. We determined the stable and unstable regions using frequency-domain Floquet Hamiltonians for sinusoidal variations, and complemented the analysis by analytical determination of the EP contours by using piecewise constant Hamiltonians.

Compared with single harmonic models, we observe richer dynamics and have more control over the regions of broken \mathcal{PT} symmetry. There are in total only three arrangements of drives with nontrivial Floquet quasienergies. Although the phase diagrams of Floquet quasienergies obtained have a lot of similarities with single driving, there are some novel properties. A particular property that emerges when we have driving with different frequencies, is the additional observation of the interlacing of wisps or resonances of the two different harmonics. When we introduce a Hermitian drive into an anti-Hermitian driven system, wisps from the phase diagram do not merge at finite driving strength, γ . Furthermore, by studying the Berry phases arising from adiabatic cyclic evolution, we find complex structures with non-Hermitian models. Non-Hermiticity brings about an imaginary part to the Berry phases, and in different regions of the Hamiltonian's instantaneous eigenvalues, the behavior of the complex Berry phase for \mathcal{PT} -symmetric and \mathcal{AP} -symmetric models is markedly different.

We can classify our models into two categories. All our models have a static Hermitian term and we complement it either with two anti-Hermitian or one Hermitian plus one anti-Hermitian periodic driving. The latter is experimentally more easily implemented, particularly in the semiclassical or quantum platforms where both gain-loss Z drive and the Hermitian Y drive are tunable [31,32,35,49,50,52]. The former, corresponding to gain-loss Y and Z drives, is challenging: the first one corresponds to the Hatano-Nelson model [67] while the second one corresponds to the “standard” gain-loss dimer case. However, non-Hermitian Floquet engineering offers a way to implement both Y and Z anti-Hermitian drives [51].

A straightforward extension of this work entails replacing the Pauli operators by higher-dimensional representations of $SU(2)$ [68,69]. In the static and single-drive Floquet problems, this replacement does not qualitatively change the Floquet results, except that the degree of EPs—the number of eigenmodes that coalesce together at the degeneracy—is given by the dimensionality of the representation. Other possible extensions include irrational values of β where the total Hamiltonian $H(t)$ is only quasiperiodic.

ACKNOWLEDGMENTS

This work was supported by the U.S. Department of Energy through the LANL/LDRD Program and the Center for Nonlinear Studies. Y.N.J. acknowledges LANL's hospitality and is supported by Office of Naval Research (ONR) Grant No. N00014-21-1-2630.

[1] I. I. Rabi, Space quantization in a gyrating magnetic field, *Phys. Rev.* **51**, 652 (1937).

[2] J. H. Shirley, Solution of the Schrödinger equation with a Hamiltonian periodic in time, *Phys. Rev.* **138**, B979 (1965).

- [3] T. Dittrich, P. Hänggi, G.-L. Ingold, B. Kramer, G. Schön, and W. Zwerger, *Quantum Transport and Dissipation* (Wiley-VCH, Weinheim, 1998), pp. 249–286.
- [4] G. E. Santoro, Introduction to Floquet Lecture notes, SISSA, Trieste (2019), https://www.ggi.infn.it/sft/SFT_2019/LectureNotes/Santoro.pdf.
- [5] T. Oka and S. Kitamura, Floquet engineering of quantum materials, *Annu. Rev. Condens. Matter Phys.* **10**, 387 (2019).
- [6] T. Kitagawa, E. Berg, M. Rudner, and E. Demler, Topological characterization of periodically driven quantum systems, *Phys. Rev. B* **82**, 235114 (2010).
- [7] N. Lindner, G. Refael, and V. Galitski, Floquet topological insulator in semiconductor quantum wells, *Nat. Phys.* **7**, 490 (2011).
- [8] M. Rechtsman, J. Zeuner, Y. Plotnik, Y. Lumer, D. Podolsky, F. Dreisow, S. Nolte, M. Segev, and A. Szameit, Photonic Floquet topological insulators, *Nature (London)* **496**, 196 (2013).
- [9] H. Lignier, C. Sias, D. Ciampini, Y. Singh, A. Zenesini, O. Morsch, and E. Arimondo, Dynamical control of matter-wave tunneling in periodic potentials, *Phys. Rev. Lett.* **99**, 220403 (2007).
- [10] M. Jiang, H. Su, Z. Wu, X. Peng, and D. Budker, Floquet maser, *Sci. Adv.* **7**, eabe0719 (2021).
- [11] C. M. Bender and S. Boettcher, Real spectra in non-Hermitian Hamiltonians having \mathcal{PT} -symmetry, *Phys. Rev. Lett.* **80**, 5243 (1998).
- [12] C. M. Bender, S. Boettcher, and P. N. Meisinger, \mathcal{PT} -Symmetric quantum mechanics, *J. Math. Phys.* **40**, 2201 (1999).
- [13] Y. N. Joglekar, C. Thompson, D. D. Scott, and G. Vemuri, Optical waveguide arrays: Quantum effects and \mathcal{PT} -symmetry, *Eur. Phys. J. Appl. Phys.* **63**, 30001 (2013).
- [14] C. M. Bender, D. C. Brody, and H. F. Jones, Complex extension of quantum mechanics, *Phys. Rev. Lett.* **89**, 270401 (2002).
- [15] A. Mostafazadeh, Pseudo-Hermiticity versus \mathcal{PT} symmetry: The necessary condition for the reality of the spectrum of a non-Hermitian Hamiltonian, *J. Math. Phys.* **43**, 205 (2002).
- [16] A. Mostafazadeh, Exact \mathcal{PT} -symmetry is equivalent to Hermiticity, *J. Phys. A: Math. Gen.* **36**, 7081 (2003).
- [17] A. Mostafazadeh, Pseudo-Hermitian representation of quantum mechanics, *Int. J. Geom. Methods Mod. Phys.* **07**, 1191 (2010).
- [18] M. Znojil, Special Issue “Pseudo-Hermitian Hamiltonians in quantum physics in 2014”, *Int. J. Theor. Phys.* **54**, 3867 (2015).
- [19] R. El-Ganainy, K. Makris, D. Christodoulides, and Z. H. Musslimani, Theory of coupled optical \mathcal{PT} -symmetric structures, *Opt. Lett.* **32**, 2632 (2007).
- [20] S. Klaiman, U. Günther, and N. Moiseyev, Visualization of branch points in \mathcal{PT} -symmetric waveguides, *Phys. Rev. Lett.* **101**, 080402 (2008).
- [21] A. Guo, G. J. Salamo, D. Duchesne, R. Morandotti, M. Volatier-Ravat, V. Aimez, G. A. Siviloglou, and D. N. Christodoulides, Observation of \mathcal{PT} -symmetry breaking in complex optical potentials, *Phys. Rev. Lett.* **103**, 093902 (2009).
- [22] C. E. Rüter, K. G. Makris, R. El-Ganainy, D. N. Christodoulides, M. Segev, and D. Kip, Observation of parity–time symmetry in optics, *Nat. Phys.* **6**, 192 (2010).
- [23] Z. Lin, H. Ramezani, T. Eichelkraut, T. Kottos, H. Cao, and D. N. Christodoulides, Unidirectional invisibility induced by \mathcal{PT} -symmetric periodic structures, *Phys. Rev. Lett.* **106**, 213901 (2011).
- [24] J. Schindler, A. Li, M. C. Zheng, F. M. Ellis, and T. Kottos, Experimental study of active LRC circuits with \mathcal{PT} symmetries, *Phys. Rev. A* **84**, 040101(R) (2011).
- [25] T. Wang, J. Fang, Z. Xie, N. Dong, Y. N. Joglekar, Z. Wang, J. Li, and L. Luo, Observation of two \mathcal{PT} transitions in an electric circuit with balanced gain and loss, *Eur. Phys. J. D* **74**, 167 (2020).
- [26] M. A. Quiroz-Juárez, K. S. Agarwal, Z. A. Cochran, J. L. Aragón, Y. N. Joglekar, and R. de J. León-Montiel, On-demand parity-time symmetry in a lone oscillator through complex synthetic gauge fields, *Phys. Rev. Appl.* **18**, 054034 (2022).
- [27] A. Regensburger, C. Bersch, M.-A. Miri, G. Onishchukov, D. N. Christodoulides, and U. Peschel, Parity–time synthetic photonic lattices, *Nature (London)* **488**, 167 (2012).
- [28] C. M. Bender, B. K. Berntson, D. Parker, and E. Samuel, Observation of \mathcal{PT} phase transition in a simple mechanical system, *Am. J. Phys.* **81**, 173 (2013).
- [29] L. Chang, X. Jiang, S. Hua, C. Yang, J. Wen, L. Jiang, G. Li, G. Wang, and M. Xiao, Parity–time symmetry and variable optical isolation in active–passive-coupled microresonators, *Nat. Photonics* **8**, 524 (2014).
- [30] X. Zhu, H. Ramezani, C. Shi, J. Zhu, and X. Zhang, \mathcal{PT} -symmetric acoustics, *Phys. Rev. X* **4**, 031042 (2014).
- [31] Y. Wu, W. Liu, J. Geng, X. Song, X. Ye, C.-K. Duan, X. Rong, and J. Du, Observation of parity-time symmetry breaking in a single-spin system, *Science* **364**, 878 (2019).
- [32] M. Naghiloo, M. Abbasi, Y. N. Joglekar, and K. W. Murch, Quantum state tomography across the exceptional point in a single superconducting qubit, *Nat. Phys.* **15**, 1232 (2019).
- [33] W. Chen, M. Abbasi, Y. N. Joglekar, and K. W. Murch, Quantum jumps in the non-Hermitian dynamics of a superconducting qubit, *Phys. Rev. Lett.* **127**, 140504 (2021).
- [34] W. Chen, M. Abbasi, B. Ha, S. Erdamar, Y. N. Joglekar, and K. W. Murch, Decoherence-induced exceptional points in a dissipative superconducting qubit, *Phys. Rev. Lett.* **128**, 110402 (2022).
- [35] L. Ding, K. Shi, Q. Zhang, D. Shen, X. Zhang, and W. Zhang, Experimental determination of \mathcal{PT} -symmetric exceptional points in a single trapped ion, *Phys. Rev. Lett.* **126**, 083604 (2021).
- [36] L. Ge and H. E. Türeci, Antisymmetric \mathcal{PT} -photonic structures with balanced positive- and negative-index materials, *Phys. Rev. A* **88**, 053810 (2013).
- [37] P. Peng, W. Cao, C. Shen, W. Qu, J. Wen, L. Jiang, and Y. Xiao, Anti-parity-time symmetry with flying atoms, *Nat. Phys.* **12**, 1139 (2016).
- [38] X.-L. Zhang, T. Jiang, and C. T. Chan, Dynamically encircling an exceptional point in anti-parity-time symmetric systems: Asymmetric mode switching for symmetry-broken modes, *Light Sci. Appl.* **8**, 88 (2019).
- [39] Y. Jiang, Y. Mei, Y. Zuo, Y. Zhai, J. Li, J. Wen, and S. Du, Anti-parity-time symmetric optical four-wave mixing in cold atoms, *Phys. Rev. Lett.* **123**, 193604 (2019).
- [40] Q. Li, C.-J. Zhang, Z.-D. Cheng, W.-Z. Liu, J.-F. Wang, F.-F. Yan, Z.-H. Lin, Y. Xiao, K. Sun, Y.-T. Wang, J.-S. Tang, J.-S. Xu, C.-F. Li, and G.-C. Guo, Experimental simulation of anti-parity-time symmetric Lorentz dynamics, *Optica* **6**, 67 (2019).
- [41] Y. Li, Y.-G. Peng, L. Han, M.-A. Miri, W. Li, M. Xiao, X.-F. Zhu, J. Zhao, A. Alu, S. Fan, and C.-W. Qiu, Anti-parity-time symmetry in diffusive systems, *Science* **364**, 170 (2019).

- [42] J. Cen and A. Saxena, Anti- \mathcal{PT} -symmetric qubit: Decoherence and entanglement entropy, *Phys. Rev. A* **105**, 022404 (2022).
- [43] A. S. Rodrigues, R. M. Ross, V. V. Konotop, A. Saxena, and P. G. Kevrekidis, Nonlinear anti-(parity-time) symmetric dimer, *Front. Phys.* **10**, 865910 (2022).
- [44] L. Ding, K. Shi, Y. Wang, Q. Zhang, C. Zhu, L. Zhang, J. Yi, S. Zhang, X. Zhang, and W. Zhang, Information retrieval and eigenstate coalescence in a non-Hermitian quantum system with anti- \mathcal{PT} symmetry, *Phys. Rev. A* **105**, L010204 (2022).
- [45] J. Bian, P. Lu, T. Liu, H. Wu, X. Rao, K. Wang, Q. Lao, Y. Liu, F. Zhu, and L. Luo, Quantum simulation of a general anti- \mathcal{PT} -symmetric Hamiltonian with a trapped ion qubit, *Fundam. Res.* **3**, 904 (2023).
- [46] Y. N. Joglekar, R. Marathe, P. Durganandini, and R. K. Pathak, \mathcal{PT} spectroscopy of the Rabi problem, *Phys. Rev. A* **90**, 040101(R) (2014).
- [47] T. E. Lee and Y. N. Joglekar, \mathcal{PT} -symmetric Rabi model: Perturbation theory, *Phys. Rev. A* **92**, 042103 (2015).
- [48] X. Luo, J. Huang, H. Zhong, X. Qin, Q. Xie, Y. S. Kivshar, and C. Lee, Pseudo-parity-time symmetry in optical systems, *Phys. Rev. Lett.* **110**, 243902 (2013).
- [49] J. Li, A. K. Harter, J. Liu, L. de Melo, Y. N. Joglekar, and L. Luo, Observation of parity-time symmetry breaking transitions in a dissipative Floquet system of ultracold atoms, *Nat. Commun.* **10**, 855 (2019).
- [50] W. Liu, Y. Wu, C.-K. Duan, X. Rong, and J. Du, Dynamically encircling an exceptional point in a real quantum system, *Phys. Rev. Lett.* **126**, 170506 (2021).
- [51] A. Kumar, K. W. Murch, and Y. N. Joglekar, Maximal quantum entanglement at exceptional points via unitary and thermal dynamics, *Phys. Rev. A* **105**, 012422 (2022).
- [52] M. Abbasi, W. Chen, M. Naghiloo, Y. N. Joglekar, and K. W. Murch, Topological quantum state control through exceptional-point proximity, *Phys. Rev. Lett.* **128**, 160401 (2022).
- [53] M. Chitsazi, H. Li, F. M. Ellis, and T. Kottos, Experimental realization of Floquet \mathcal{PT} -symmetric systems, *Phys. Rev. Lett.* **119**, 093901 (2017).
- [54] R. de J. León-Montiel, M. A. Quiroz-Juárez, J. L. Domínguez-Juárez, R. Quintero-Torres, J. L. Aragón, A. K. Harter, and Y. N. Joglekar, Observation of slowly decaying eigenmodes without exceptional points in Floquet dissipative synthetic circuits, *Commun. Phys.* **1**, 88 (2018).
- [55] H. Kazemi, M. Y. Nada, T. Mealy, A. F. Abdelshafy, and F. Capolino, Exceptional points of degeneracy induced by linear time-periodic variation, *Phys. Rev. Appl.* **11**, 014007 (2019).
- [56] H. Kazemi, M. Y. Nada, A. Nikzamir, F. Maddaleno, and F. Capolino, Experimental demonstration of exceptional points of degeneracy in linear time periodic systems and exceptional sensitivity, *J. Appl. Phys.* **131**, 144502 (2022).
- [57] H. R. K. Park, J. Jeon, G. Y. Cho, and S. B. Lee, Controllable Floquet edge modes in a multifrequency driving system, *Phys. Rev. B* **107**, 085141 (2023).
- [58] K. Sandholzer, A.-S. Walter, J. Minguzzi, Z. Zhu, K. Viebahn, and T. Esslinger, Floquet engineering of individual band gaps in an optical lattice using a two-tone drive, *Phys. Rev. Res.* **4**, 013056 (2022).
- [59] M. V. Berry, Quantal phase factors accompanying adiabatic changes, *Proc. R. Soc. Lond. A* **392**, 45 (1984).
- [60] J. W. Zwanziger, M. Koenig, and A. Pines, Berry's phase, *Annu. Rev. Phys. Chem.* **41**, 601 (1990).
- [61] J. J. Sakurai and J. Napolitano, *Modern Quantum Mechanics*, 2nd ed. (Cambridge University Press, Cambridge, 2017), pp. 348–355.
- [62] A. K. Harter and Y. N. Joglekar, Connecting active and passive \mathcal{PT} -symmetric Floquet modulation models, *Prog. Theor. Exp. Phys.* **2020**, 12A106 (2020).
- [63] G. Dattoli, R. Mignani, and A. Torre, Geometrical phase in the cyclic evolution of non-Hermitian systems, *J. Phys. A: Math. Gen.* **23**, 5795 (1990).
- [64] N. A. Sinitsyn and A. Saxena, Geometric phase for non-Hermitian Hamiltonian evolution as anholonomy of a parallel transport along a curve, *J. Phys. A: Math. Theor.* **41**, 392002 (2008).
- [65] R. Hayward and F. Biancalana, Complex Berry phase dynamics in \mathcal{PT} -symmetric coupled waveguides, *Phys. Rev. A* **98**, 053833 (2018).
- [66] B. Lu, X.-F. Liu, Y.-P. Gao, C. Cao, T.-J. Wang, and C. Wang, Berry phase in an anti- \mathcal{PT} symmetric metal-semiconductor complex system, *Opt. Express* **27**, 22237 (2019).
- [67] N. Hatano and D. R. Nelson, Localization transitions in non-Hermitian quantum mechanics, *Phys. Rev. Lett.* **77**, 570 (1996).
- [68] M. A. Quiroz-Juárez, A. Perez-Leija, K. Tschernig, B. M. Rodríguez-Lara, Omar S. Magaña-Loaiza, K. Busch, Y. N. Joglekar, and R. J. León-Montiel, Exceptional points of any order in a single, lossy waveguide beam splitter by photon-number-resolved detection, *Photon. Res.* **7**, 862 (2019).
- [69] Z. Bian, L. Xiao, K. Wang, X. Zhan, F. Assogba Onanga, F. Ruzicka, W. Yi, Y. N. Joglekar, and P. Xue, Conserved quantities in parity-time symmetric systems, *Phys. Rev. Res.* **2**, 022039(R) (2020).